BNL-229699-2026-TECH
CA/AP/746

Estimating Residual Gas Beam Loss in the BNL AGS Booster:Model, Numerical Tools, and Implications for a Polarimeter Chamber

F. Rathmann

April 2026

Collider Accelerator Department
Brookhaven National Laboratory

U.S. Department of Energy
USDOE Office of Science (SC), Nuclear Physics (NP)

DISCLAIMER

Estimating Residual Gas Beam Loss in the BNL AGS Booster

Model, Numerical Tools, and Implications for a Polarimeter Chamber

Frank Rathmann

April 16, 2026

Abstract

Beam loss from residual gas scattering is calculated for a storage ring of circumference $C = 200\,\mathrm{m}$, covering a linear magnetic rigidity ramp from $B\rho_{\mathrm{inj}} = 1.25\,\mathrm{T\,m}$ to $B\rho_{\mathrm{ext}} = 9.50\,\mathrm{T\,m}$ over $t_{\mathrm{ramp}} = 1.00\,\mathrm{s}$. Three loss mechanisms are considered: nuclear inelastic reactions, single Coulomb scattering beyond the acceptance angle of the machine, and charge-state exchange for heavy ions. Calculations are performed for protons and Au^{32+} ions, the latter being the charge state delivered by the EBIS pre-injector into the BNL AGS Booster. At a baseline vacuum of $P_0 = 5 \times 10^{-11}\,\mathrm{mbar}$ the integrated fractional beam loss over the full ramp is negligible for protons ($< 0.001\%$) and 33.1% for Au^{32+}. The impact of a 1 m polarimeter section at elevated pressure $P_s = 5 \times 10^{-9}\,\mathrm{mbar}$ is evaluated: the proton loss remains negligible, while the Au^{32+} loss rises to 45.1%, establishing the vacuum requirement for the polarimeter chamber. In the present compact approximate model, Au^{32+} losses are dominated by charge exchange at injection, while proton losses are dominated by single Coulomb scattering. The design, outgassing budget, pumping strategy, and commissioning sequence for a UHV polarimeter chamber housing silicon detectors and ASICs are described in detail.

1 Overview

Beam particles circulating in a storage ring undergo collisions with molecules of the residual gas in the vacuum chamber. Three mechanisms contribute to particle loss:

1. nuclear inelastic (hadronic) reactions,
2. single Coulomb scattering beyond the acceptance angle of the ring, and
3. charge exchange (relevant for heavy ions).

The instantaneous fractional loss rate (s^{-1}) is

$$\frac{1}{\tau} = \sum_g \sum_k \bar{n}_g \, \sigma_{k,g} \, \beta c, \tag{1}$$

where the outer sum runs over gas species g, the inner sum over loss mechanisms k, $\bar{n}_g$ is the effective number density of species g averaged around the ring, $\sigma_{k,g}$ is the relevant cross section, and βc is the beam velocity.

Effective number density with a special section

If a section of length ℓ has a local pressure P_s while the remainder of the circumference C has baseline pressure P_0, the effective density for species g with fractional composition f_g is

$$\bar{n}_g = f_g \left[n(P_0) \, \frac{C - \ell}{C} + n(P_s) \, \frac{\ell}{C} \right], \tag{2}$$

where, assuming ideal gas at room temperature $T = 300\,\mathrm{K}$,

$$n(P) = \frac{P}{k_B T}. \tag{3}$$

Pressures are expressed in mbar; 1 mbar = 100 Pa. Throughout this document the special section is assumed to have the same gas composition as the rest of the ring (see Table 1), differing only in its local pressure P_s. This is a conservative assumption appropriate for a polarimeter chamber that is not differentially pumped to a different gas species mix.

Table 1: Residual gas composition assumed for the UHV environment modeled as a mixture of four gas species in the ring and the special section.

Species	Z_g	Fraction f_g
H_2	2	0.75
CO	14	0.10
N_2	14	0.10
CO_2	22	0.05

2 Relativistic kinematics

The beam is characterized by its magnetic rigidity $B\rho$ (T·m). For a particle with charge number Z_b and rest mass m_0, the momentum is

$$p = Z_b\, e\, B\rho, \tag{4}$$

from which the Lorentz factors follow,

$$\gamma = \sqrt{1 + \left(\frac{pc}{m_0 c^2}\right)^2}, \qquad \beta = \frac{pc}{\gamma\, m_0 c^2}. \tag{5}$$

The kinetic energy per nucleon is $T/A = (\gamma - 1)\, m_0 c^2/A$.

3 Cross-section parametrizations

3.1 Nuclear inelastic reactions

The total nuclear reaction cross section is represented here by a compact geometric approximation based on the Bradt–Peters radius-sum picture of nuclear reactions [1]. In the present note this is written as

$$\sigma_{\mathrm{nuc}}(A_b, A_g) = 0.83\, \pi r_0^2 \left(A_b^{1/3} + A_g^{1/3}\right)^2, \tag{6}$$

where A_b and A_g are the mass numbers of the beam particle and gas nucleus, respectively, and $r_0 = 1.36\,\mathrm{fm}$. More elaborate semi-empirical reaction-cross-section parametrizations, such as the Sihver form used in transport codes including Geant4, introduce an additional overlap or transparency correction to this geometric radius-sum expression [2, 3]. In the present compact model, that correction is approximated by the constant factor 0.83, treated as an empirical reduction relative to the naive black-disk estimate. This simplified form is retained because nuclear inelastic reactions are a subleading contribution in the present beam-loss model, and the dominant dependence is the geometric scaling with nuclear size.

3.2 Single Coulomb scattering

A particle deflected beyond the acceptance angle θ_{acc} of the ring is assumed lost. In the unscreened Rutherford approximation, the laboratory-frame differential cross section is [4]

$$\frac{d\sigma}{d\Omega} = \left(\frac{Z_b Z_g \alpha \hbar c}{2\, p\beta c}\right)^2 \frac{1}{\sin^4(\theta/2)}\,. \tag{7}$$

Integrating over all scattering angles $\theta > \theta_{\mathrm{acc}}$ gives

$$\sigma_{\mathrm{Coul}}(\theta > \theta_{\mathrm{acc}}) = 2\pi \int_{\theta_{\mathrm{acc}}}^{\pi} \frac{d\sigma}{d\Omega}\, \sin\theta\, d\theta = 4\pi \left(\frac{Z_b Z_g \alpha \hbar c}{2\, p\beta c}\right)^2 \left[\frac{1}{\sin^2(\theta_{\mathrm{acc}}/2)} - 1\right]. \tag{8}$$

For $\theta_{\rm acc} \ll 1$, this reduces to

$$\sigma_{\rm Coul}(\theta > \theta_{\rm acc}) \approx \pi \left(\frac{Z_b Z_g \alpha \hbar c}{p\beta c \, \sin(\theta_{\rm acc}/2)} \right)^2 . \tag{9}$$

An acceptance angle of $\theta_{\rm acc} = 1\,\text{mrad}$ is assumed (see Table 2). The cross section therefore scales approximately as $(p\beta)^{-2}$ and decreases rapidly during acceleration.

3.3 Charge exchange

For highly charged heavy ions, electron capture from the residual gas leads to a change in charge state and immediate loss from the stored beam. In the present note, this contribution is represented by the compact phenomenological approximation

$$\sigma_{\rm CE}(Z_b, \gamma) \approx \frac{C_{\rm CE}\, Z_b^{2.5}}{\gamma^6}, \tag{10}$$

with $C_{\rm CE} \approx 10^{-20}\,\text{cm}^2$. This form is used here as a simple upper-estimate model for heavy-ion losses: it captures the strong increase with projectile charge state, while the corresponding loss rate scales as $\beta\gamma^{-6}$ through the factor $r = n\sigma v$. Over the Booster rigidity range, the increase in beam velocity partly offsets the γ^{-6} suppression of the cross section. For protons ($Z_b = 1$), this term is taken to be negligible.

At injection ($B\rho = 1.25\,\text{T m}$, with the 1 m polarimeter section included) the total loss rate of Au^{32+} is $2.02 \times 10^{-1}\,\text{s}^{-1}$, compared to $1.80 \times 10^{-5}\,\text{s}^{-1}$ for protons. In this compact model, the Au^{32+} instantaneous loss rate at injection is dominated by charge exchange (99.9%), whereas proton losses are dominated by single Coulomb scattering.

Representativeness of Au^{32+} for Booster heavy-ion operation. The BNL Booster accelerates a range of heavy-ion species delivered by the EBIS (Electron Beam Ion Source) injector. In addition to gold, RHIC has operated with copper (Cu^{29+}, $Z = 29$, $A = 63$), aluminium (Al^{13+}), iron (Fe^{26+}), zirconium (Zr^{40+}), and ruthenium (Ru^{44+}), as well as uranium (U^{92+} or partially stripped from EBIS at $Z_b \approx 28$–32). In the compact approximate model adopted here, $\sigma_{\rm CE} \propto Z_b^{2.5}$, so uranium ($Z = 92$) has a charge-exchange cross section roughly $(92/79)^{2.5} \approx 1.5$ times larger than gold at the same γ, making it the most demanding species within this simplified scaling. All lighter species (Cu, Al, Fe, Zr, Ru) have substantially smaller Z_b and hence lower charge-exchange rates. Gold therefore sits near the top of the charge-exchange severity scale among routine RHIC species, and the vacuum requirement derived here ($P \leq 5 \times 10^{-9}\,\text{mbar}$) should be treated as a lower bound: within the present compact model, uranium operation would impose an approximately 50% tighter constraint on the tolerable loss increment from the polarimeter section.

4 Total loss rate and integrated beam loss

Inserting the cross sections into Eq. (1):

$$\frac{1}{\tau} = \beta c \sum_g \bar{n}_g \left[\sigma_{\rm nuc} + \sigma_{\rm Coul} + \sigma_{\rm CE} \right]_g , \tag{11}$$

so that the beam lifetime is τ (s), i.e. the e-folding time for exponential beam decay at constant loss rate.

During a $B\rho$ ramp from $B\rho_{\rm inj}$ to $B\rho_{\rm ext}$, all three cross sections depend on the instantaneous rigidity, so the loss rate is time-varying. For a *linear* ramp of duration $t_{\rm ramp}$,

$$B\rho(t) = B\rho_{\rm inj} + \frac{B\rho_{\rm ext} - B\rho_{\rm inj}}{t_{\rm ramp}}\, t, \tag{12}$$

so that $dt/d(B\rho) = t_{\rm ramp}/\Delta B\rho$ is constant. The beam survival at time t is

$$\frac{N(t)}{N_0} = \exp\!\left(-\int_0^t \frac{dt'}{\tau(t')}\right) = \exp\!\left(-\frac{t_{\rm ramp}}{\Delta B\rho}\int_{B\rho_{\rm inj}}^{B\rho(t)} \frac{d(B\rho')}{\tau(B\rho')}\right), \tag{13}$$

and the total fractional beam loss over the full ramp is

$$\frac{\Delta N}{N_0} = 1 - \frac{N(t_{\rm ramp})}{N_0}. \tag{14}$$

The integral is evaluated numerically by summing the areas of successive trapezoids under the curve on a dense $B\rho$ grid of 500 points spanning $B\rho_{\rm inj} = 1.25\,\mathrm{T\,m}$ to $B\rho_{\rm ext} = 9.50\,\mathrm{T\,m}$ over a ramp of $t_{\rm ramp} = 1.00\,\mathrm{s}$, at baseline pressure $P_0 = 5\times10^{-11}\,\mathrm{mbar}$.

5 Beam and machine parameters

The machine and vacuum parameters used in all calculations are collected in Table 2. The ring circumference and rigidity range correspond to the BNL AGS Booster. The baseline pressure $P_0 = 5\times10^{-11}\,\mathrm{mbar}$ and the UHV gas composition, given in Table 1, are representative of a well-baked stainless steel vacuum system. The special section models a 1 m polarimeter chamber at elevated local pressure $P_s = 5\times10^{-9}\,\mathrm{mbar}$, assuming the same gas composition as the rest of the ring; it represents 0.5% of the circumference. The acceptance angle $\theta_{\rm acc} = 1\,\mathrm{mrad}$ enters the Coulomb scattering cross section (Section 3.2) and is characteristic of the Booster lattice. The beam species are listed in Table 3; Au^{32+} is the charge state at Booster injection from the EBIS pre-injector [5]. The machine and lattice parameters adopted here are consistent with those documented for gold and uranium operation in the Booster injector chain [5, 6].

Table 2: Machine and vacuum parameters used in the calculations.

Parameter	Value
Ring circumference C	200 m
Injection rigidity $B\rho_{\rm inj}$	1.25 T m
Extraction rigidity $B\rho_{\rm ext}$	9.50 T m
Ramp duration $t_{\rm ramp}$	1.00 s (linear)
Baseline pressure P_0	5×10^{-11} mbar
Gas composition	see Table 1
Special section length ℓ	1.0 m (0.5% of C)
Special section pressure P_s	5×10^{-9} mbar (same gas composition as baseline)
Acceptance angle $\theta_{\rm acc}$	1 mrad

Table 3: Beam species parameters.

Species	Z_b	A	m_0c^2 (MeV)	Notes
Proton	1	1	938.3	
Au^{32+}	32	197	183 454	EBIS charge state at Booster injection

6 Numerical results

Table 4 summarises the instantaneous loss rates and beam lifetimes at injection ($B\rho = 1.25\,\mathrm{T\,m}$) and extraction ($B\rho = 9.50\,\mathrm{T\,m}$), together with the total fractional beam loss integrated over the 1.00 s linear ramp, for both species and both vacuum configurations (baseline and with the

1 m special section at 5×10^{-9} mbar). The dominant loss mechanism at injection is indicated in the lower rows: for protons, Coulomb scattering accounts for essentially 100% of the loss rate in the present compact model, while for Au^{32+} charge exchange contributes 99.9% and Coulomb scattering the remaining 0.1%.

Table 4: Summary of beam loss results for the parameters of Tables 2 and 3. Baseline: uniform $P_0 = 5 \times 10^{-11}$ mbar. Special section: $\ell = 1$ m at $P_s = 5 \times 10^{-9}$ mbar (0.5% of circumference), same gas composition as baseline.

		w/ special section		Baseline only	
Species	Quantity	@ inj	@ ext	@ inj	@ ext
Proton	Loss rate (s^{-1})	1.798×10^{-5}	1.416×10^{-7}	1.203×10^{-5}	9.472×10^{-8}
	Lifetime τ (s)	5.562×10^{4}	7.061×10^{6}	8.314×10^{4}	1.056×10^{7}
	Integrated loss (%)	< 0.001		< 0.001	
Au^{32+}	Loss rate (s^{-1})	2.019×10^{-1}	7.195×10^{-1}	1.351×10^{-1}	4.813×10^{-1}
	Lifetime τ (s)	4.954	1.390	7.414	2.078
	Integrated loss (%)	45.1		33.1	
@ inj	Proton	Nuclear 0.0%	Coulomb 100.0%	Charge exchange 0.0%	
	Au^{32+}	Nuclear 0.0%	Coulomb 0.1%	Charge exchange 99.9%	

Figures 1–3 show the corresponding plots. The discussion follows the natural sequence of the calculation: instantaneous rates first, mechanism breakdown second, and finally the integrated beam survival over the full ramp.

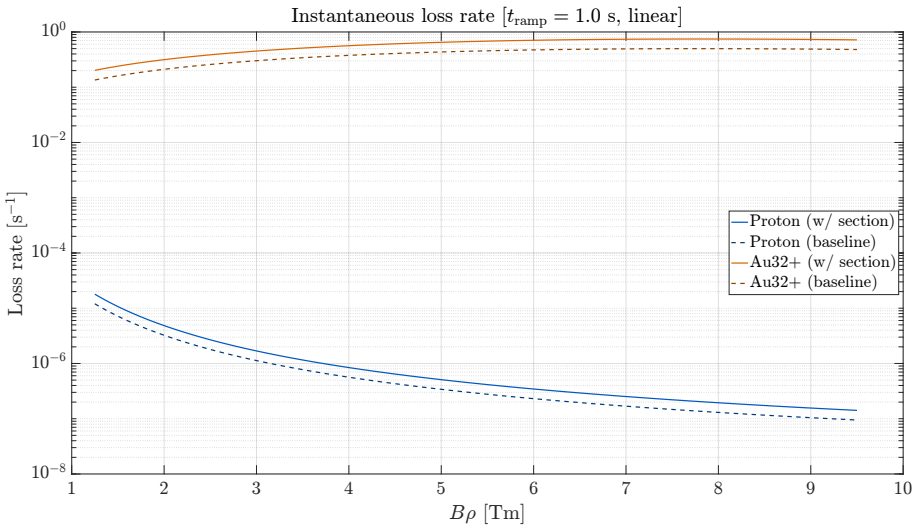

Figure 1: Instantaneous loss rate $1/\tau$ as a function of magnetic rigidity $B\rho$ for protons and Au^{32+}, computed for the parameters of Tables 2 and 3. Solid lines include the 1 m special section at 5×10^{-9} mbar; dashed lines show the uniform baseline. Both axes are logarithmic. In the adopted compact charge-exchange model, the Au^{32+} loss rate scales as $\beta\gamma^{-6}$; over the Booster rigidity range, the increase in beam velocity outweighs the modest γ^{-6} suppression, so the Au^{32+} rate rises with increasing $B\rho$. At injection the Au^{32+} rate is dominated by charge exchange, while the proton rate is dominated by Coulomb scattering.

7 Polarimeter vacuum system: design and commissioning

The polarimeter chamber must operate at $P_s \leq 5 \times 10^{-9}$ mbar to limit additional Au^{32+} beam loss during heavy-ion Booster operation (Section 6; see in particular Fig. 2 for the mechanism

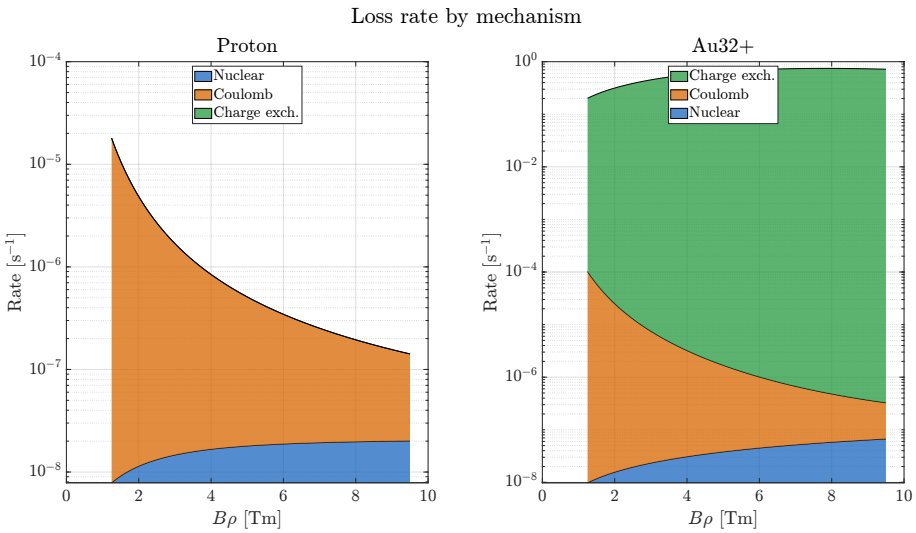

Figure 2: Loss rate by mechanism (nuclear inelastic, Coulomb scattering, charge exchange) as a function of $B\rho$, shown as a stacked area plot for protons (left) and Au^{32+} (right), for the parameters of Tables 2 and 3 with the special section included. For protons, single Coulomb scattering (essentially 100% at injection) dominates throughout the ramp, with nuclear inelastic reactions contributing only a negligible residual component. For Au^{32+} ($Z_b = 32$), the loss rate is dominated by charge exchange at injection in the present compact model; over the Booster rigidity range the charge-exchange loss rate rises because the factor β in $r = n\sigma v$ increases faster than the adopted γ^{-6} suppression decreases.

breakdown and Fig. 3 for the integrated loss). This section describes the vacuum system design, the outgassing budget, the pumping strategy, and the complete commissioning sequence.

7.1 Chamber geometry and outgassing budget

The polarimeter vacuum vessel is modelled as a stainless steel cylinder of length $L = 1\,\mathrm{m}$ and inner diameter $d = 50\,\mathrm{cm}$, giving a total inner surface area of

$$A = \pi dL + 2 \cdot \tfrac{\pi d^2}{4} = \pi \times 50 \times 100 + 2 \times \pi \times 25^2 \approx 19\,600\,\mathrm{cm}^2 \approx 2\,\mathrm{m}^2. \tag{15}$$

The outgassing rate q (mbar·l/s/cm^2) depends critically on the thermal history of the surface. Representative values for stainless steel are given in Table 5.

Table 5: Stainless steel outgassing rates and implied pumping speed for $P = 5 \times 10^{-9}$ mbar (polarimeter section target pressure), $A = 19\,600\,\mathrm{cm}^2$. The halving-per-10 K rule is used for intermediate bake temperatures.

Condition	q (mbar·l/s/cm^2)	$Q = qA$ (mbar·l/s)	$S = Q/P$ (l/s)
Unbaked (after $\sim 10\,\mathrm{h}$ pumping)	10^{-8}	2×10^{-4}	200 000
Baked 50 °C	$\sim 1.5 \times 10^{-9}$	3×10^{-5}	30 000
Baked 80 °C	$\sim 1.3 \times 10^{-10}$	2.5×10^{-6}	2500
Baked 150 °C	$\sim 10^{-10}$	2×10^{-6}	2000
Baked 250 °C	$\sim 10^{-12}$	2×10^{-8}	20

Baking to 250 °C reduces the required pumping speed by four orders of magnitude relative to the unbaked case, making a 250 °C bake of the bare chamber an essential step rather than an optional one. A 50 °C bake alone leaves the required speed at $\sim 30\,000\,\mathrm{l/s}$, which is impractical. The 250 °C bake must therefore be performed on the bare chamber *before* detector installation.

7.2 Silicon detectors and ASICs in vacuum

Silicon sensors are inherently vacuum-compatible. The challenge lies in the associated readout electronics. Standard printed circuit board (PCB) materials (FR4 glass-fibre laminate), plastic

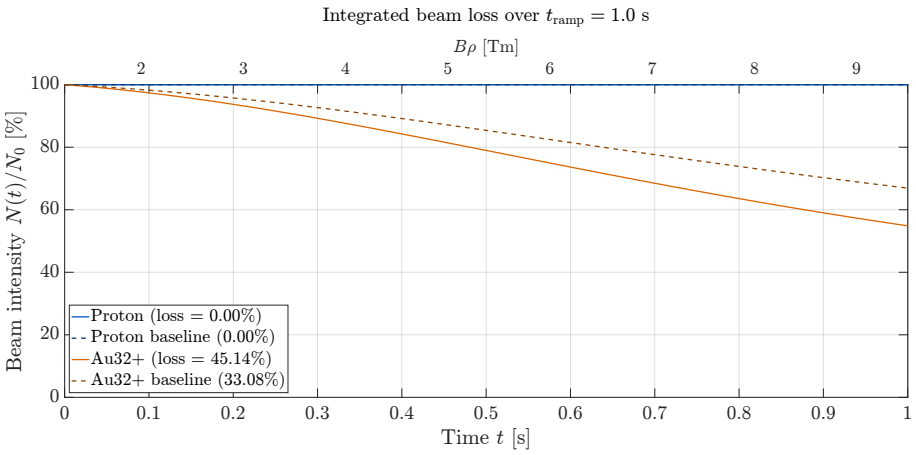

Figure 3: Beam survival $N(t)/N_0$ during the 1.00 s linear ramp for the parameters of Tables 2 and 3. The upper x-axis shows the corresponding magnetic rigidity. Solid lines include the 1 m special section at 5×10^{-9} mbar; dashed lines show the uniform baseline. The proton beam loss is below 0.001% over the full ramp in both vacuum configurations. The Au^{32+} beam loses 45.1% (with special section) or 33.1% (baseline), with charge exchange dominating the heavy-ion loss budget throughout the ramp in the present compact model.

connectors, and organic adhesives outgas at rates orders of magnitude above the vacuum budget and must be entirely eliminated. The adopted solution is a ceramic hybrid module approach:

- **Substrate**: aluminium nitride (AlN) ceramic with Direct Bond Copper (DBC) metallisation, a process in which copper layers are bonded directly to the ceramic surface without adhesive. AlN offers thermal conductivity of 170 W/m K (compared to 20 W/m K for Al_2O_3), a coefficient of thermal expansion (CTE) of 4.5 ppm/K close to silicon (3 ppm/K), and an outgassing rate of $< 10^{-12}$ mbar·l/s/cm^2, negligible in the context of the chamber wall.
- **ASIC**: radiation-hard application-specific integrated circuit (ASIC) wire-bonded to the ceramic substrate. Power dissipation must be < 1 W per module to remain within the capacity of the conductive cooling path to the chamber flange (see Thermal path below).
- **Adhesives**: vacuum-grade epoxy only. EPO-TEK H20E[1] (silver-filled, electrically conductive) is used for die attachment; LOCTITE STYCAST 2850FT[2] (thermally conductive, mechanically stable) for structural bonds. No standard solder flux; all solder joints cleaned thoroughly after reflow.
- **Capacitors**: bare ceramic chip capacitors attached with vacuum-grade conductive epoxy. C0G (NP0) dielectric is used for precision signal-path capacitors; its capacitance is stable to within ±30 ppm/K and independent of applied voltage. X7R dielectric, whose capacitance varies by up to ±15% relative to its nominal value over the temperature range −55 °C to 125 °C, is acceptable for bypass and decoupling where exact capacitance is not critical. No plastic-encapsulated components.
- **Signal routing**: Kapton flex cable from detector module to vacuum feedthrough. All-metal ceramic-to-metal feedthroughs (D-subminiature or custom multi-pin) through the chamber wall. Leak rate $< 10^{-10}$ mbar·l/s per feedthrough.
- **Thermal path**: heat is conducted from the ASIC, e.g., via a copper stud → flexible copper braid strap → water-cooled copper block on the chamber flange. Target thermal resistance < 10 K/W from junction to coolant.

[1] EPO-TEK H20E, Meridian Adhesives, https://meridianadhesives.com/products/epo-tek-h20e/.

[2] LOCTITE STYCAST 2850FT, Henkel Adhesives, https://www.henkel-adhesives.com/ng/en/product/potting-compounds/loctite_stycast_2850ftblk.html.

The maximum safe bake temperature for the fully assembled detector module is 80 °C, limited by epoxy joint reliability and wire-bond fatigue caused by the differential thermal expansion between silicon and ceramic (CTE mismatch) during heating cycles. The assembled system is therefore baked to 50 °C as a conservative margin, primarily to drive off residual solvents from epoxy joints and moisture adsorbed during installation.

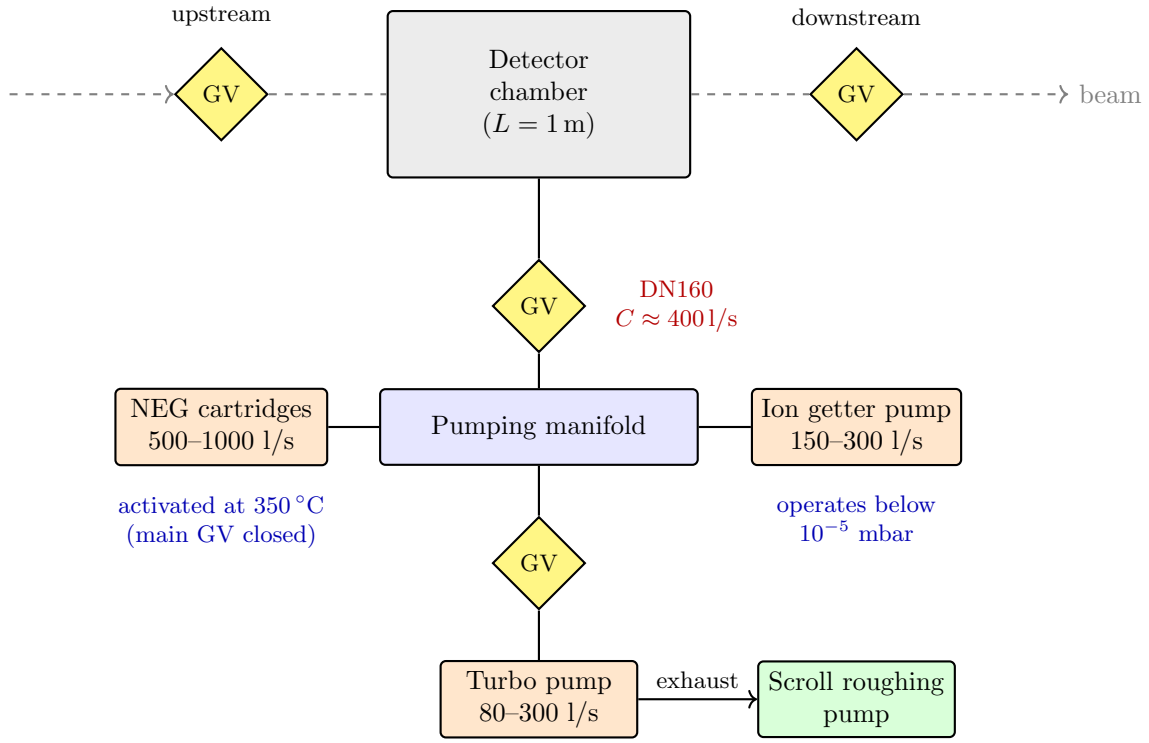

Figure 4: Schematic of the polarimeter vacuum system (not to scale). Upstream and downstream gate valves (GV) isolate the detector chamber from the beam line. The main DN160 gate valve ($C \approx 400$ l/s) connects the chamber to the pumping manifold, which carries the NEG cartridges and the ion getter pump. A separate gate valve isolates the turbomolecular pump, used only for initial pump-down and bakeout and valved off during steady-state operation. NEG activation (350 °C) is performed with the main DN160 gate valve closed to protect the detectors.

7.3 Pumping system

The pumping system, schematically shown in Fig. 4, combines three complementary technologies:

Turbomolecular pump Used during initial pump-down and baking phases. Effective for all gas species; required to reach $\sim 10^{-6}$ mbar before the ion getter pump can start. Valved off during steady-state operation. Typical size: 80 l/s–300 l/s.

Non-evaporable getter (NEG) cartridges Pump H_2, H_2O, CO, CO_2, and N_2 by chemisorption, the dominant residual gas species after baking. Completely passive during operation (no power required). Must be activated by heating to 350 °C in vacuum prior to use. Typical effective speed for H_2: 500 l/s–1000 l/s per cartridge. Cannot pump noble gases or methane.

Ion getter pump Pumps all gas species including noble gases (which NEG cannot address) by ionisation and burial in a titanium cathode. No moving parts; vibration-free; fully bakeable. Operates only below $\sim 10^{-5}$ mbar. Provides continuous pressure monitoring via pump current. Typical size: 150 l/s–300 l/s.

The NEG cartridges and ion getter pump are mounted on a common pumping port separated from the detector chamber by a large-bore gate valve (DN160 recommended). This arrangement allows NEG activation at 350 °C with the gate valve closed and detectors fully protected, and

permits future NEG regeneration without venting the detector chamber.

The conductance of the gate valve limits the effective pumping speed seen by the chamber:

$$\frac{1}{S_{\text{eff}}} = \frac{1}{S_{\text{pump}}} + \frac{1}{C_{\text{valve}}}, \tag{16}$$

where $C_{\text{valve}} \approx 150\,\text{l/s}$ for a DN100 valve and $\approx 400\,\text{l/s}$ for DN160. For a 1000 l/s NEG behind a DN160 gate valve:

$$S_{\text{eff}} = \left(\frac{1}{1000} + \frac{1}{400}\right)^{-1} \approx 290\,\text{l/s}, \tag{17}$$

which comfortably exceeds the 20 l/s required after the 250 °C bake, with ample margin to accommodate surface recontamination during the dry-N_2 vent and detector installation.

7.4 Commissioning Strategy

The commissioning of the polarimeter vacuum system follows a four-phase strategy that reflects the changing material inventory of the chamber and the corresponding thermal constraints.

Phase 1 ⟶ Phase 2 ⟶ Phase 3 ⟶ Phase 4

The vacuum-system layout relevant for this procedure is shown in Fig. 4. The logic of the sequence is summarized in Table 6, while the full detailed step-by-step procedure is deferred to Appendix A.

Table 6: Summary of the four-phase commissioning strategy for the polarimeter vacuum system. The detailed numbered sequence is given in Appendix A.

Phase	Purpose	Main actions	Target / constraint
1	Bare-chamber preparation	Assemble stainless-steel chamber without detectors or other temperature-sensitive components; perform the high-temperature bake; activate the NEG cartridges.	Pressure in low-10^{-10} mbar range before detector installation.
2	Detector installation	Isolate chamber, vent only with high-purity dry nitrogen, install detectors, cables, and feedthroughs, then pump down again and reconnect to activated NEG and ion pump.	No exposure to air; minimize chamber open time.
3	Post-installation conditioning	Carry out moderate-temperature bake of fully assembled system and allow pressure to recover under active pumping.	Nominal bake at 50 °C, strict upper limit 80 °C; final pressure at or below 5×10^{-9} mbar.
4	Steady-state operation	Operate with NEG cartridges and ion getter pump active, keep full pumping path available to chamber, and monitor vacuum performance continuously.	Main gate valve open during normal running; ion pump current used as pressure proxy.

The sequence is deliberately irreversible in the favorable direction. The bare chamber is first brought to true UHV condition by high-temperature treatment and NEG activation, after which detector installation is carried out under dry-N_2 conditions in a controlled and limited departure from that state. Once detector modules, ASICs, cables, and epoxy-bonded components are installed, the system can no longer tolerate the temperatures required for full chamber degassing or getter activation. Vacuum recovery must then rely on clean handling, rapid pump-down, moderate-temperature conditioning, and continuous passive pumping.

The key rules that govern this strategy are simple. First, the initial 250 °C bake and NEG activation must be completed before detector installation. Second, after the bare-chamber bake the detector volume must never be vented with air; only high-purity dry nitrogen is acceptable. Third, once the detector hardware is installed, the chamber temperature must never exceed 80 °C, with 50 °C taken as the nominal post-installation bake temperature. Finally, any accidental air exposure after completion of Phase 1 would return the chamber to a substantially higher outgassing state and would require repetition of the full preparation cycle from the beginning.

7.5 Operation with a Carbon-Fiber Target

Operation with the carbon-fiber target is foreseen only for polarized beam species. In that case, the relevant beams are light ions, for which the residual-gas-induced loss constraints are much less severe than for heavy-ion Booster operation. The vacuum requirements during carbon-target operation therefore do not need to be driven by the same considerations that dominate the heavy-ion case discussed above.

By contrast, during heavy-ion running the residual-gas contribution to beam loss is a central design constraint, and the presence of the carbon target itself, together with its support structure and associated outgassing load, should not be allowed to compromise the chamber vacuum. The design should therefore provide a dedicated parking or "garage" position for the carbon-fiber target behind a UHV gate valve, so that the target installation and preparation can be fully isolated from the Booster polarimeter chamber whenever operation with heavy ions is required.

The operational concept is thus a clean separation of modes. For heavy-ion running, the carbon target remains retracted and isolated behind the UHV valve, preserving the vacuum conditions required when residual-gas effects are important. For polarized light-ion running, the valve can be opened and the target inserted into the beam line as needed for polarimetry measurements. In this way, the demanding vacuum requirements of heavy-ion operation can be maintained without sacrificing the functionality of the carbon-target polarimeter for polarized beams.

8 Conclusion

A self-consistent model of residual-gas beam loss has been developed for a storage ring with circumference $C = 200\,\mathrm{m}$, covering the full magnetic rigidity range from injection ($B\rho = 1.25\,\mathrm{T\,m}$) to extraction ($B\rho = 9.50\,\mathrm{T\,m}$). Three loss mechanisms, namely nuclear inelastic reactions, single Coulomb scattering, and charge exchange, are parameterized using a combination of standard and phenomenological cross-section parametrizations and integrated numerically over a 1.00 s linear ramp.

The key findings are:

- **Protons** lose less than 0.001% of the beam over the full ramp at baseline pressure $P_0 = 5 \times 10^{-11}\,\mathrm{mbar}$, dominated throughout by Coulomb scattering with a small nuclear inelastic contribution. Adding the 1 m polarimeter section at $P_s = 5 \times 10^{-9}\,\mathrm{mbar}$ leaves the integrated loss at the same negligible level.
- **$\mathbf{Au}^{32+}$** loses 33.1% (baseline) or 45.1% (with polarimeter section) over the ramp. In the compact approximate model used here, charge exchange dominates the instantaneous loss rate at injection and remains the key driver of the integrated heavy-ion loss. Although the adopted charge-exchange cross section scales as γ^{-6}, the corresponding loss rate is proportional to $\beta\gamma^{-6}$; over the Booster rigidity range, the increase in beam velocity outweighs the modest γ^{-6} suppression, so the charge-exchange loss rate rises with increasing $B\rho$.
- The **polarimeter vacuum requirement** is $P_s = 5 \times 10^{-9}\,\mathrm{mbar}$, which adds about 12.1 percentage points to the Au^{32+} integrated loss (from 33.1% to 45.1%). Meeting this target after detector installation requires a 250 °C bake of the bare chamber prior to detector insertion, reducing the required pumping speed by four orders of magnitude to $\approx 20\,\mathrm{l/s}$.

- The **pumping strategy**: NEG cartridges (500–1000 l/s) combined with an ion getter pump (150–300 l/s), separated from the detector chamber by a DN160 gate valve ($C \approx 400$ l/s), provides an effective speed of ≈ 290 l/s, well in excess of the post-bake requirement and with ample margin for surface recontamination during detector installation.
- The **commissioning sequence** in four phases (bare-chamber bake, detector installation under dry-N_2, post-installation bake to 50 °C, steady-state operation) is designed to be irreversible in the correct direction: each phase degrades gracefully, and unintended air exposure at any point after Phase 1 requires a full restart rather than a partial recovery.

The MATLAB script, `ring_loss_calculator_v9_final.m` in Appendix B, has been used to produce the numerical results in this document and can be used directly to evaluate the impact of changes to ring parameters, vacuum pressure, ramp duration, or beam species.

References

[1] H. L. Bradt and B. Peters. The heavy nuclei of the primary cosmic radiation. *Physical Review*, 77(1):54–70, 1950. doi:10.1103/PhysRev.77.54.

[2] L. Sihver, C. H. Tsao, R. Silberberg, T. Kanai, and A. F. Barghouty. Total reaction and partial cross section calculations in proton-nucleus ($z_t \leq 26$) and nucleus-nucleus reactions (z_p and $z_t \leq 26$). *Physical Review C*, 47(3):1225–1236, 1993. doi:10.1103/PhysRevC.47.1225.

[3] Geant4 Collaboration. *Geant4 Physics Reference Manual*, release 10.4 edition, 2017. Chapter 5, Hadronic Physics, nucleus-nucleus cross sections; Sihver formula. URL: https://geant4.web.cern.ch/documentation/pipelines/master/prm_html/PhysicsReferenceManual/.

[4] E. Rutherford. Lxxix. the scattering of α and β particles by matter and the structure of the atom. *The London, Edinburgh, and Dublin Philosophical Magazine and Journal of Science*, 21(125):669–688, 1911. URL: https://www.tandfonline.com/doi/abs/10.1080/14786440508637080, doi:10.1080/14786440508637080.

[5] C. J. Gardner. FY2016 parameters for gold ions in Booster, AGS, and RHIC. Technical Report C-A/AP Note 574, Brookhaven National Laboratory, October 2016. URL: https://www.bnl.gov/isd/documents/94091.pdf.

[6] C. J. Gardner. Parameters for the injection, acceleration, and extraction of uranium ions in Booster, AGS, and RHIC. Technical Report C-A/AP Note 474, Brookhaven National Laboratory, November 2012. URL: https://www.bnl.gov/isd/documents/79594.pdf.

A Detailed Commissioning Sequence

For completeness, the full step-by-step commissioning procedure corresponding to the summary given in Section 7.4 is listed below.

Phase 1: Bare-chamber bake

1. Assemble the stainless-steel chamber with pumping manifold, gate valve, and pumping package, but without detectors, Kapton cables, or other temperature-sensitive organic components.
2. Bake the chamber uniformly to 250 °C while pumping continuously with the turbomolecular pump.
3. Activate the NEG cartridges separately by local heating to about 350 °C, with the chamber isolated by the gate valve if required by the thermal layout.
4. Continue pumping until the pressure reaches the low-10^{-10} mbar range. If this is not achieved, extend the bake or check for leaks or insufficiently degassed components.

Phase 2: Dry-N_2 venting and detector installation

1. After successful completion of the initial bake and NEG activation, isolate the chamber from the pumping package by closing the main gate valve.
2. Vent the chamber exclusively with high-purity dry nitrogen. Venting with laboratory air must be avoided.
3. Install the silicon detector modules, Kapton flex cables, feedthroughs, and associated internal hardware under dry-nitrogen conditions. Keep the chamber open time as short as reasonably possible.
4. After closure, pump down again with the roughing and turbomolecular pumps to the 10^{-5} mbar range, then reopen the gate valve so that the chamber is again connected to the activated NEG cartridges and ion getter pump.

Phase 3: Post-installation low-temperature bake

1. Once detectors, ASICs, cables, and other temperature-sensitive components are installed, high-temperature baking is no longer permissible.
2. Perform a second bake at about 50 °C, with a strict upper limit of 80 °C, for at least 48 h while maintaining active pumping.
3. A temporary pressure rise is expected as weakly bound adsorbates are released, followed by a gradual decrease as the chamber approaches its operating condition.
4. After cooldown to room temperature, verify that the chamber pressure stabilizes at or below the design target of about 5×10^{-9} mbar.

Phase 4: Steady-state operation

1. During beam operation the chamber vacuum is maintained primarily by the activated NEG cartridges together with the ion getter pump.
2. The turbomolecular pump remains available as a valved backup for recovery or diagnostics.
3. The main gate valve between chamber and pumping package should remain open during normal operation so that the full effective pumping speed is continuously available.
4. The ion pump current should be monitored as a proxy for chamber pressure and as a diagnostic of slow drifts or abnormal vacuum excursions.

Key Rules

1. The initial 250 °C bake and NEG activation must be completed before detector installation.

2. After completion of the bare-chamber bake, the detector chamber must never be vented with air. Only high-purity dry nitrogen may be used.
3. After detector installation, the chamber temperature must never exceed 80 °C; the nominal post-installation bake temperature is about 50 °C.
4. Any accidental exposure to ambient air after the initial conditioning would return the chamber to a much higher outgassing state and would require repetition of the full preparation sequence from the beginning.

B Appendix: MATLAB Implementation

The numerical results presented in this note were generated with the MATLAB script `ring_loss_calculator_v9_final.m`, reproduced below for completeness. The script requires MATLAB R2016b or later for local functions and MATLAB R2020a or later for `exportgraphics`. To repeat the calculation for a different machine, vacuum, or beam species, edit the PARAMETERS block in lines 109–129 and then run the full script, either with `F5` or from the MATLAB Command Window via `>> ring_loss_calculator_v9_final`.

```
%% ring_loss_calculator_v9_final.m
% ========================================================================
% Residual Gas Beam Loss in a Storage Ring
% Instantaneous loss rate and integrated fractional beam loss over a
% linear magnetic rigidity ramp.
%
% Author:  Frank Rathmann
% Date:    April 2026
% Version: 9
%
% Associated publication:
%   F. Rathmann, "Estimating Residual Gas Beam Loss in the BNL AGS
%   Booster: Model, Numerical Tools, and Implications for a Polarimeter
%   Chamber", BNL Technical Note (2026).
%
% ------------------------------------------------------------------------
% Physics model
% ------------------------------------------------------------------------
% Three loss mechanisms are included:
%
%  1. Nuclear inelastic reactions
%     Compact geometric estimate:
%       sigma_nuc = 0.83 * pi * r0^2 * (Ab^(1/3) + At^(1/3))^2
%     with r0 = 1.36 fm.
%
%     IMPORTANT:
%     This is kept intentionally as a compact approximate model. The factor
%     0.83 is treated here as an empirical reduction of the pure geometric
%     radius-sum estimate. It is not the full Sihver overlap correction.
%
%  2. Single Coulomb scattering beyond machine acceptance angle theta_acc
%     Rutherford cross section integrated above theta_acc:
%       sigma_Coul(theta > theta_acc)
%         = 4*pi * (Zb*Zg*alpha*hbar*c / (2*p*beta*c))^2
%             * [ 1/sin^2(theta_acc/2) - 1 ]
%
%     For small theta_acc this reduces to the familiar 1/sin^2(theta/2)
%     scaling. The old 1/sin^4(theta/2) form was too strong by two powers
```

```
%     of sin(theta/2).
%
%  3. Charge-state exchange (phenomenological upper-estimate model)
%     Compact approximate scaling:
%       sigma_CE = C_CE * Zb^2.5 / gamma^6
%       with C_CE ~ 1e-20 cm^2
%
%     IMPORTANT:
%     We intentionally revert here to the original compact form rather than
%     the more detailed Schlachter-type reduced-variable scaling. For the
%     present beam-loss note this is used as a simple phenomenological model
%     that tends to preserve an upper estimate of heavy-ion losses. Protons
%     (Zb <= 1) are taken to have negligible charge-exchange loss.
%
% Instantaneous fractional loss rate:
%   1/tau = sum_g n_eff(g) * [sigma_nuc + sigma_Coul + sigma_CE] * beta*c
%
% where n_eff(g) is the effective number density of species g, weighted by
% the fraction of circumference at each pressure:
%   n_eff(g) = f_g * [ n(P0)*(C-ell)/C + n(Ps)*ell/C ]
% with n(P) = P/(kB*T) for ideal gas at T = 300 K.
%
% ------------------------------------------------------------------------
% Ramp model and integration
% ------------------------------------------------------------------------
% Linear ramp: Brho(t) = Brho_inj + (Brho_ext - Brho_inj) * t / t_ramp
% => dt/dBrho = t_ramp / Delta_Brho  (constant)
%
% Beam survival:
%   N(t)/N0 = exp( -integral_0^t dt'/tau(t') )
%           = exp( -(t_ramp/Delta_Brho) * cumtrapz(Brho, 1/tau(Brho)) )
%
% Integrated fractional loss:
%   Delta_N/N0 = 1 - N(t_ramp)/N0
%
% The integral is evaluated by the trapezoidal rule (MATLAB cumtrapz)
% on a uniform Brho grid of N_points steps.
%
% ------------------------------------------------------------------------
% Usage
% ------------------------------------------------------------------------
% Edit the PARAMETERS section below, then run the full script (F5 or
% >> ring_loss_calculator_v9_final in the Command Window).
% Do NOT run individual sections (Ctrl+Enter) in isolation.
%
% Outputs:
%   Command window : summary table (loss rates, lifetimes, integrated
%                    losses, mechanism fractions at injection)
%   Figure 1       : instantaneous loss rate vs Brho  (semi-log)
%   Figure 2       : beam survival N(t)/N0 vs time    (linear)
%   Figure 3       : loss rate by mechanism vs Brho   (stacked area, log)
%   PDF files      : fig1_loss_rate.pdf, fig2_beam_intensity.pdf,
%                    fig4_mechanisms.pdf  (exported via exportgraphics)
% ========================================================================

clear; clc; close all;

set(0, 'DefaultTextInterpreter',          'latex');
```

```
set(0, 'DefaultAxesTickLabelInterpreter', 'latex');
set(0, 'DefaultLegendInterpreter',        'latex');
set(0, 'DefaultAxesFontName',             'Times');

%% PHYSICAL CONSTANTS (do not edit)
c_light = 2.99792458e8;   % speed of light (m/s)
mp      = 938.272e6;      % proton rest mass energy (eV)
u_mass  = 931.494e6;      % atomic mass unit energy (eV)
kB      = 1.38065e-23;    % Boltzmann constant (J/K)
MBAR2PA = 100.0;          % unit conversion: 1 mbar = 100 Pa
T_gas   = 300;            % residual gas temperature (K)

%% PARAMETERS (edit here)

% Ring geometry and ramp
C        = 200;   % ring circumference (m)
Brho_inj = 1.25;  % injection magnetic rigidity (Tm)
Brho_ext = 9.5;   % extraction magnetic rigidity (Tm)
t_ramp   = 1.0;   % linear ramp duration (s)

% Baseline vacuum
P_base = 5e-11;   % baseline residual gas pressure (mbar)

% Special section (e.g. polarimeter chamber)
sec_length   = 1.0;   % length of special section (m)
sec_pressure = 5e-9;  % local pressure in section (mbar)
sec_enabled  = true;  % true = include section; false = uniform baseline

% Machine acceptance half-angle (enters Coulomb cross section)
theta_acc = 1e-3;     % acceptance half-angle (rad)

% Numerical resolution
N_points = 500;       % Brho grid points

%% PLOT COLOURS (do not edit unless desired)
% Row 1: nuclear, Row 2: Coulomb, Row 3: charge exchange
mech_colors = [0.10 0.40 0.75;
               0.85 0.40 0.00;
               0.15 0.60 0.25];

%% RESIDUAL GAS COMPOSITION
% Compact approximate treatment:
% gas.Z and gas.A are treated as effective molecular target parameters.
%
% This is exact neither for nuclear reactions nor for charge exchange, but
% it keeps the model compact and applies the same species bookkeeping
% consistently to all three loss mechanisms.
gas.name = {'H2', 'CO',  'N2',  'CO2'};
gas.Z    = [2,    14,    14,    22  ];   % effective target charge
gas.A    = [2,    28,    28,    44  ];   % effective target mass number
gas.frac = [0.75, 0.10,  0.10,  0.05];   % volume fractions, sum = 1

%% BEAM SPECIES
beam(1).name  = 'Proton';
beam(1).Z     = 1;
beam(1).A     = 1;
beam(1).m0    = mp;
beam(1).color = [0.00, 0.35, 0.75];
```

```
155
156 % Au32+ is the EBIS charge state injected into the BNL AGS Booster.
157 beam(2).name  = 'Au32+';
158 beam(2).Z     = 32;                % charge state, not atomic number 79
159 beam(2).A     = 197;
160 beam(2).m0    = 197 * u_mass;      % neglect electron binding energy
161 beam(2).color = [0.85, 0.40, 0.00];
162
163 %% DERIVED VECTORS
164 Brho_vec = linspace(Brho_inj, Brho_ext, N_points);
165 t_vec    = linspace(0, t_ramp, N_points);
166 dBrho_dt = (Brho_ext - Brho_inj) / t_ramp;
167
168 %% MAIN CALCULATION
169 results   = struct();
170 results_b = struct();
171
172 for ib = 1:2
173
174     % Loss profile with the special section included
175     [rate, tau, r_nuc, r_cou, r_ce, gam_v, bet_v] = ...
176         compute_profile(beam(ib), Brho_vec, P_base, ...
177                         sec_length, C, sec_pressure, sec_enabled, ...
178                         gas, kB, MBAR2PA, T_gas, c_light, theta_acc);
179
180     % Loss profile for the uniform baseline case
181     [rate_b, tau_b, ~, ~, ~, ~, ~] = ...
182         compute_profile(beam(ib), Brho_vec, P_base, ...
183                         sec_length, C, P_base, false, ...
184                         gas, kB, MBAR2PA, T_gas, c_light, theta_acc);
185
186     % Ramp integration in Brho space
187     integrand   = (1 ./ tau)   / dBrho_dt;
188     integrand_b = (1 ./ tau_b) / dBrho_dt;
189
190     cum_int   = cumtrapz(Brho_vec, integrand);
191     cum_int_b = cumtrapz(Brho_vec, integrand_b);
192
193     N_norm   = exp(-cum_int);
194     N_norm_b = exp(-cum_int_b);
195
196     frac_loss   = 1 - N_norm(end);
197     frac_loss_b = 1 - N_norm_b(end);
198
199     results(ib).rate      = rate;
200     results(ib).tau       = tau;
201     results(ib).nuc       = r_nuc;
202     results(ib).cou       = r_cou;
203     results(ib).ce        = r_ce;
204     results(ib).gamma     = gam_v;
205     results(ib).beta      = bet_v;
206     results(ib).N_norm    = N_norm;
207     results(ib).frac_loss = frac_loss;
208
209     results_b(ib).rate      = rate_b;
210     results_b(ib).tau       = tau_b;
211     results_b(ib).N_norm    = N_norm_b;
212     results_b(ib).frac_loss = frac_loss_b;
```

```
end

%% SUMMARY TABLE
fprintf('\n======================================================================\n');
fprintf(' STORAGE RING BEAM LOSS SUMMARY\n');
fprintf(' C = %.0f m | Brho: %.2f -> %.2f Tm | t_ramp = %.2f s (linear)\n', ...
        C, Brho_inj, Brho_ext, t_ramp);
fprintf(' P_base = %.1e mbar\n', P_base);
fprintf(' theta_acc = %.3e rad (%.3f mrad)\n', theta_acc, 1e3*theta_acc);
fprintf(' Gas composition:');
for ig = 1:length(gas.name)
    fprintf(' %s %.0f%%', gas.name{ig}, 100*gas.frac(ig));
end
fprintf('\n');
if sec_enabled
    fprintf(' Special section: %.1f m at %.1e mbar, same gas (%.3f%% of ring)\n', ...
            sec_length, sec_pressure, 100*sec_length/C);
end
fprintf('======================================================================\n');
fprintf(' %-8s %-13s %-13s %-13s %-13s\n', ...
        'Species','Rate@inj(1/s)','Rate@ext(1/s)','tau@inj(s)','tau@ext(s)');
fprintf(' %s\n', repmat('-',1,64));
for ib = 1:2
    fprintf(' %-8s %-13.3e %-13.3e %-13.3e %-13.3e\n', ...
        beam(ib).name, ...
        results(ib).rate(1), results(ib).rate(end), ...
        results(ib).tau(1),  results(ib).tau(end));
end

fprintf('\n Integrated fractional loss over %.2f s ramp\n', t_ramp);
fprintf(' %-8s %-25s %-25s\n', 'Species', 'w/ special section (%)', 'baseline (%)');
fprintf(' %s\n', repmat('-',1,64));
for ib = 1:2
    fprintf(' %-8s %-25.3f %-25.3f\n', ...
        beam(ib).name, ...
        100*results(ib).frac_loss, ...
        100*results_b(ib).frac_loss);
end

fprintf('\n Beam lifetimes in convenient units:\n');
fprintf(' %-8s %-28s %-28s\n', 'Species', ...
        'w/ special section (inj / ext)', 'baseline (inj / ext)');
fprintf(' %s\n', repmat('-',1,82));
for ib = 1:2
    fprintf(' %-8s %-28s %-28s\n', ...
        beam(ib).name, ...
        sprintf('%s / %s', format_lifetime(results(ib).tau(1)),   format_lifetime(
    results(ib).tau(end))), ...
        sprintf('%s / %s', format_lifetime(results_b(ib).tau(1)), format_lifetime(
    results_b(ib).tau(end))));
end

fprintf('\n Mechanism fractions at injection (w/ special section):\n');
for ib = 1:2
    tot = results(ib).rate(1);
    fprintf(' %-8s: Nuclear %5.1f%% Coulomb %5.1f%% ChargeExch %5.1f%%\n', ...
        beam(ib).name, ...
        100*results(ib).nuc(1)/tot, ...
```

```
        100*results(ib).cou(1)/tot, ...
        100*results(ib).ce(1)/tot);
end
fprintf('================================================================\n\n');

%% FIGURE 1: INSTANTANEOUS LOSS RATE vs Brho
figure(1); clf;
set(gcf, 'Color','w', 'Name','Instantaneous Loss Rate', ...
         'Position',[50 500 700 400]);
for ib = 1:2
    semilogy(Brho_vec, results(ib).rate, '-', ...
             'Color', beam(ib).color, 'LineWidth', 2.2, ...
             'DisplayName', [beam(ib).name ' (w/ section)']);
    hold on;
    if sec_enabled
        semilogy(Brho_vec, results_b(ib).rate, '--', ...
                 'Color', beam(ib).color*0.65, 'LineWidth', 2.2, ...
                 'DisplayName', [beam(ib).name ' (baseline)']);
    end
end
grid on; box on;
xlabel('$B\rho$ [Tm]', 'FontSize', 36);
ylabel('Loss rate [s$^{-1}$]', 'FontSize', 36);
title(sprintf('Instantaneous loss rate [$t_\\mathrm{ramp} = %.1f$ s, linear]', t_ramp), ...
      'FontSize', 36);
legend('Location','east', 'FontSize', 30);
set(gca, 'FontSize', 33);

%% FIGURE 2: BEAM SURVIVAL N(t)/N0 vs TIME
figure(2); clf;
set(gcf, 'Color','w', 'Name','Beam Survival During Ramp', ...
         'Position',[760 500 750 560]);

ax1 = axes('Position', [0.13 0.11 0.75 0.55]);
for ib = 1:2
    plot(ax1, t_vec, 100*results(ib).N_norm, '-', ...
         'Color', beam(ib).color, 'LineWidth', 2.2, ...
         'DisplayName', sprintf('%s (loss = %.2f\\%%)', ...
                                beam(ib).name, 100*results(ib).frac_loss));
    hold(ax1, 'on');
    if sec_enabled
        plot(ax1, t_vec, 100*results_b(ib).N_norm, '--', ...
             'Color', beam(ib).color*0.65, 'LineWidth', 2.2, ...
             'DisplayName', sprintf('%s baseline (%.2f\\%%)', ...
                                    beam(ib).name, 100*results_b(ib).frac_loss));
    end
end
grid(ax1, 'on'); box(ax1, 'on');
xlabel(ax1, 'Time $t$ [s]', 'FontSize', 36);
ylabel(ax1, 'Beam intensity $N(t)/N_0$ [\%]', 'FontSize', 36);
legend(ax1, 'Location','southwest', 'FontSize', 30);
ylim(ax1, [0 100]);
set(ax1, 'FontSize', 33);

ax2 = axes('Position', ax1.Position, ...
           'XAxisLocation','top', 'YAxisLocation','right', ...
           'Color','none', 'YTick',[], 'Box','off');
```

```
ax2.XLim = [Brho_inj Brho_ext];
ax2.YLim = [0 100];
ax2.FontSize = 30;
xlabel(ax2, '$B\rho$ [Tm]', 'FontSize', 30);
title(ax2, sprintf('Integrated beam loss over $t_\\mathrm{ramp} = %.1f$ s', t_ramp),
    ...
      'FontSize', 33, 'Units','normalized', 'Position',[0.5, 1.18, 0]);
axes(ax1);

%% FIGURE 3: LOSS RATE BY MECHANISM vs Brho
figure(3); clf;
set(gcf, 'Color','w', 'Name','Loss Rate by Mechanism', ...
         'Position',[760 60 700 360]);
for ib = 1:2
    subplot(1,2,ib);
    h = area(Brho_vec, ...
             [results(ib).nuc(:), results(ib).cou(:), results(ib).ce(:)], ...
             'FaceAlpha', 0.75);
    h(1).FaceColor = mech_colors(1,:);
    h(2).FaceColor = mech_colors(2,:);
    h(3).FaceColor = mech_colors(3,:);
    set(gca, 'YScale','log', 'FontSize', 30);
    xlabel('$B\rho$ [Tm]', 'FontSize', 33);
    ylabel('Rate [s$^{-1}$]', 'FontSize', 33);
    title(beam(ib).name, 'FontSize', 36);
    legend({'Nuclear', 'Coulomb', 'Charge exch.'}, ...
           'Location','north', 'FontSize', 27);
    grid on; box on;
end
sgtitle('Loss rate by mechanism', 'FontSize', 39);

%% EXPORT FIGURES
try
    exportgraphics(figure(1), 'fig1_loss_rate.pdf',      'ContentType','vector');
    exportgraphics(figure(2), 'fig2_beam_intensity.pdf', 'ContentType','vector');
    exportgraphics(figure(3), 'fig4_mechanisms.pdf',     'ContentType','vector');
    fprintf('Figures exported successfully.\n');
catch ME
    fprintf('Warning: figure export failed | %s\n', ME.message);
end

%% LOCAL FUNCTIONS

function [rate, tau, r_nuc, r_cou, r_ce, gamma_v, beta_v] = ...
    compute_profile(bm, Brho_vec, P_base, sec_len, C, sec_P, sec_on, ...
                    gas, kB, MBAR2PA, T_gas, c_light, theta_acc)
% COMPUTE_PROFILE Instantaneous beam loss rate at each Brho point.
%
% The three microscopic cross sections are evaluated species by species and
% then converted to loss rates through n_eff * sigma * v.

    N = length(Brho_vec);
    rate    = zeros(1,N);
    r_nuc   = zeros(1,N);
    r_cou   = zeros(1,N);
    r_ce    = zeros(1,N);
    gamma_v = zeros(1,N);
    beta_v  = zeros(1,N);
```

```
383
384     n0 = num_density(P_base, kB, MBAR2PA, T_gas);
385     ns = num_density(sec_P,  kB, MBAR2PA, T_gas);
386     if ~sec_on
387         ns = n0;
388     end
389
390     base_frac = (C - sec_len) / C;
391     sec_frac  = sec_len / C;
392
393     for i = 1:N
394         [gam, bet, p_eVc] = kinematics(Brho_vec(i), bm);
395         v = bet * c_light;
396         gamma_v(i) = gam;
397         beta_v(i)  = bet;
398
399         rr = 0; rn = 0; rc = 0; rx = 0;
400         for ig = 1:length(gas.Z)
401             n_eff = gas.frac(ig) * (n0 * base_frac + ns * sec_frac);
402
403             sn = sigma_nuclear(bm.A, gas.A(ig));                          % m^2
404             sc = sigma_coulomb(bm.Z, gas.Z(ig), p_eVc, bet, theta_acc); % m^2
405             sx = sigma_ce(bm.Z, gam);                                     % m^2
406
407             rr = rr + n_eff * (sn + sc + sx) * v;
408             rn = rn + n_eff * sn * v;
409             rc = rc + n_eff * sc * v;
410             rx = rx + n_eff * sx * v;
411         end
412
413         rate(i)  = rr;
414         r_nuc(i) = rn;
415         r_cou(i) = rc;
416         r_ce(i)  = rx;
417     end
418
419     tau = 1 ./ rate;
420 end
421
422 function [gamma, beta, p_eVc] = kinematics(Brho, bm)
423 % KINEMATICS Relativistic kinematics from magnetic rigidity.
424 % p*c [eV] = Z * c * Brho, with Brho in Tm.
425     p_eVc = bm.Z * 299792458 * Brho;
426     gamma = sqrt(1 + (p_eVc / bm.m0)^2);
427     beta  = p_eVc / (gamma * bm.m0);
428 end
429
430 function n = num_density(P_mbar, kB, MBAR2PA, T)
431 % NUM_DENSITY Ideal-gas number density from pressure.
432     n = (P_mbar * MBAR2PA) / (kB * T);
433 end
434
435 function s = sigma_nuclear(Ap, At)
436 % SIGMA_NUCLEAR Compact approximate nuclear reaction cross section.
437 %
438 % We deliberately keep the simple geometric model
439 %   sigma = 0.83 * pi * r0^2 * (Ap^(1/3) + At^(1/3))^2
440 % rather than the full Sihver overlap correction.
```

```
%
% This is appropriate for a compact, transparent beam-loss model.
    r0 = 1.36e-15;   % m
    s  = 0.83 * pi * r0^2 * (Ap^(1/3) + At^(1/3))^2;
end

function s = sigma_coulomb(Zb, Zg, p_eVc, beta, theta_acc)
% SIGMA_COULOMB Rutherford cross section integrated above theta_acc.
%
% Exact angular integration gives
%   sigma = 4*pi*A^2 * [1/sin^2(theta_acc/2) - 1]
% with
%   A = Zb*Zg*(alpha*hbar*c)/(2*p*beta*c).
%
% alpha*hbar*c = 1.44 MeV fm is used here.
    p_MeV = p_eVc / 1e6;                % MeV/c
    sh    = sin(theta_acc / 2);
    A_fm  = (Zb * Zg * 1.44) / (2 * p_MeV * beta);  % fm
    s     = 4 * pi * (A_fm * 1e-15)^2 * (1 / sh^2 - 1);
end

function s = sigma_ce(Zb, gamma)
% SIGMA_CE Compact phenomenological charge-exchange cross section.
%
% We intentionally keep the original approximate form
%   sigma = C_CE * Zb^2.5 / gamma^6
% with
%   C_CE ~ 1e-20 cm^2.
%
% This compact model is retained here because the goal of the note is an
% honest but simple upper-estimate description of heavy-ion beam loss, not a
% species-by-species detailed capture calculation.
%
% Inputs:
%   Zb     projectile charge state
%   gamma  Lorentz factor
%
% Output:
%   s      charge-exchange cross section in m^2
%
% Protons:
%   For Zb <= 1 the capture-loss channel is taken to be negligible.
    if Zb <= 1
        s = 0;
        return;
    end

    C_CE_cm2 = 1e-20;                % cm^2
    s = C_CE_cm2 * Zb^2.5 / gamma^6;  % cm^2
    s = s * 1e-4;                    % convert cm^2 -> m^2
end

function txt = format_lifetime(tau_s)
% FORMAT_LIFETIME Return beam lifetime in a convenient human-readable unit.
    if tau_s < 60
        txt = sprintf('%.2f s', tau_s);
    elseif tau_s < 3600
        txt = sprintf('%.2f min', tau_s/60);
```

```
499     elseif tau_s < 86400
500         txt = sprintf('%.2f h', tau_s/3600);
501     else
502         txt = sprintf('%.2f d', tau_s/86400);
503     end
504 end
```

Listing 1: MATLAB script `ring_loss_calculator_v9_final.m`. The PARAMETERS block in lines 109–129 can be edited to adapt the calculation to a different ring, vacuum scenario, or beam species.